ESR and capacitance monitoring of a dc-link capacitor used in a three-phase PWM inverter with a front-end diode rectifier

6 blank lines
space before title (please, remove these comment lines in the submitted version)

ESR and capacitance monitoring of a dc-link capacitor used in a three-phase PWM inverter with a front-end diode rectifier

1 line space

K. Hasegawa[a,*], S. Nishizawa[b], I. Omura[a]

1 line space

[a] *Department of Biological Functions Engineering, Kyushu Institute of Technology, 2-4, Hibikino, Wakamatsu-ku, Kitakyushu, Fukuoka, 808-0196, Japan*
[b] *Research Institute for Applied Mechanics, Kyushu University 6-1 Kasuga-koen, Kasuga, Fukuoka, 816-8580, Japan*

2 lines space

Abstract

Condition monitoring plays an important role in estimating health condition of capacitors because the ageing of the capacitors is usually accompanied by an increase in equivalent series resistance (ESR) and a decrease in capacitance. Either capacitance or ESR cannot be a unique indicator of the lifetime of capacitors in some cases. This paper presents a condition monitoring method of a dc-link capacitor used in a three-phase PWM inverter with a front-end diode rectifier intended for motor drives. The monitoring method extracts both the ESR and capacitance of a capacitor under test from the actual ripple current and voltage without disconnecting the capacitor nor injecting an additional current. The monitoring method, therefore, can be implemented online. Experimental results verify that the monitoring method independently obtains the ESR and capacitance changes of the capacitor under test. This contributes to accurate lifetime estimation of dc-link capacitors.

1 line space

*** Corresponding author**
hasegawa@life.kyutech.ac.jp
Tel: +81-93-695-6059

ESR and capacitance monitoring of a dc-link capacitor used in a three-phase PWM inverter with a front-end diode rectifier

1 line space

K. Hasegawa[a], S. Nishizawa[b], I. Omura[a]

1 line space
2 lines space

2 lines space

1. Introduction

Three-phase pulse-width modulated (PWM) inverters with a front-end diode rectifier are widely used in motor drives without regenerative braking. Their DC-link capacitors act as an energy buffer to compensate for the instantaneous power difference between the rectifier and the inverter.

The DC-link capacitors, however, are a major factor in degrading the reliability because they usually have a shorter lifetime and higher failure rate than semiconductor and magnetic devices [1]. Reference [2] provides a survey of reliability in power electronic converters, which describes that the capacitors were chosen by 18% of fragile components responsible for converter failure.

Condition monitoring plays an important role in estimating health condition of power electronic converters including their capacitors [3-11]. Ageing of the capacitors is usually accompanied by an increase in equivalent series resistance (ESR) and a decrease in capacitance [12-15].

The authors of this paper have revealed that either capacitance or ESR is not always a unique indicator of the lifetime of aluminum electrolytic capacitors [16], where an ageing test of the capacitors was carried out. The test has confirmed that a higher dc-bias voltage brings a faster increase in ESR but results in a slower drop in capacitance in a range less than the rated voltage. This result implies that the estimated lifetime by the ESR is different from that by the capacitance. Hence, both the capacitance and ESR measurements are necessary for condition monitoring.

This paper proposed a condition monitoring method of a dc-link capacitor used in a three-phase inverter with a front-end diode rectifier for motor drives. The proposed method independently extracts the capacitance and ESR without disconnecting the capacitor nor injecting an additional current.

2. Ripple current flowing into a dc-link capacitor

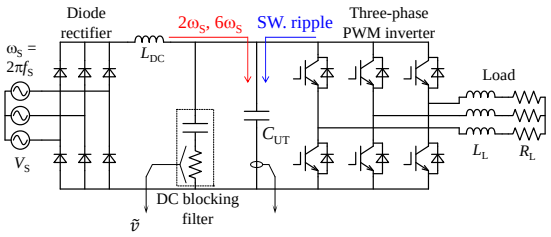

Fig. 1 Three-phase PWM inverter with a front-end diode rectifier used for experiment, indicating ripple current flowing out of the diode rectifier and the inverter.

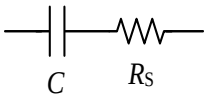

Fig. 2 Equivalent circuit of the capacitor for analysis

in three-phase PWM inverter with a front-end diode rectifier

2.1. Circuit configuration

Fig. 1 shows a three-phase PWM inverter with a front-end diode rectifier used for experiment. The diode rectifier provides the sixth harmonic of the line frequency, $6\omega_S$, in theory, and also generates the second harmonic, $2\omega_S$, in practice due to an imbalance of the three-phase line voltage or impedance. The three-phase inverter provides switching ripple current that contains the switching frequency and its multiple components. As a result, the ripple current contains multiple frequency components in a wide frequency range. This helps monitor the ESR and capacitance as discussed later.

2.2. Voltage and current sensing

This paper introduces a dc blocking filter into sensing of the capacitor voltage because the capacitor voltage contains a dc component that is much larger than the ripple component. This allows to utilize a lower voltage sensor and improves the resolution of voltage sensing.

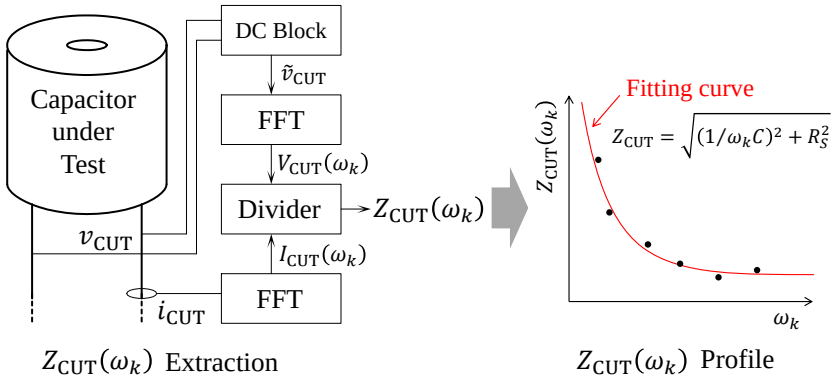

Fig. 3 Condition monitoring method that extracts both the capacitance and ESR with an impedance profile obtained from FFT results

The dc blocking filter consists of a first-order CR high-pass filter. The cutoff frequency of the filter, ω_F, is given by

$$\omega_F = \frac{1}{C_F R_F} \quad \text{[rad/s]} \qquad (1)$$

where C_F and R_F are the capacitor and resistor of the CR high-pass filter, respectively. The cutoff frequency should be larger than all the frequency components of ripple current. The minimum frequency of the ripple current is the second harmonic, $2\omega_S$, so that the cutoff frequency is designed to be larger than $2\omega_S$. This paper selects a cutoff frequency of 33 Hz (C_F = 0.47 μF, R_F = 10 kΩ) for experiment.

In designing the capacitor C_F and resistor R_F of the filter, attention should be paid to the blocking voltage of the capacitor and to the dissipated power of the resistor. The capacitor has the same blocking voltage as the dc-link capacitor has because the dc mean voltage across the capacitor is the same as that of the dc-link voltage. Since the resistor has only the ripple component, its dissipated power is greatly small.

A current sensor is installed on the negative terminal of the capacitor under test.

3. Condition monitoring method

3.1. Extraction of ESR and capacitance

Since the ripple current of the dc-link capacitor contains multiple frequency components, it can be given by [17]

$$i_{CUT} = \sum_{k=1}^{n} I_{CUT}(\omega_k)\sin(\omega_k t + \varphi_k) \qquad (2)$$

where $I_{CUT}(\omega_k)$ and ϕ_k are the amplitude and initial phase angle for each frequency, respectively.

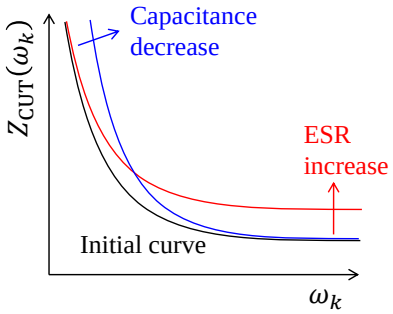

Fig. 4 Variations of the impedance profile according to capacitance or ESR change

Fig. 2 shows an equivalent circuit of the capacitor under test for this analysis, where R_S stands for the ESR of the capacitor. The voltage across the capacitor under test is given by

$$v_{CUT} = \frac{1}{C}\int i_{CUT}dt + R_S i_{CUT}$$
$$= \sum_{k=1}^{n} I_{CUT}(\omega_k)\left\{-\frac{1}{\omega_k C}\cos(\omega_k t + \varphi_k) + R_S \sin(\omega_k t + \varphi_k)\right\} \qquad (3)$$

From Equations (3), the amplitude of v_{CUT} at each frequency is given by

$$V_{CUT}(\omega_k) = I_{CUT}(\omega_k)\sqrt{\left(\frac{1}{\omega_k C}\right)^2 + R_S^2} \qquad (4)$$

Dividing (4) by $I_{CUT}(\omega_k)$ gives the impedance of the capacitor at each frequency as follows:

$$Z_{CUT}(\omega_k) = \frac{V_{CUT}(\omega_k)}{I_{CUT}(\omega_k)} = \sqrt{\left(\frac{1}{\omega_k C}\right)^2 + R_S^2} \qquad (5)$$

Equations (5) suggest that the capacitance and ESR are independently calculated if impedances at different frequencies are obtained. Multiple frequency components of the ripple current help calculate the capacitance and ESR.

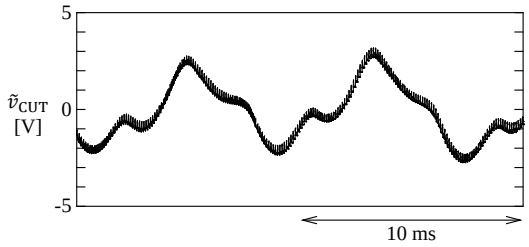

(b) Condition A.

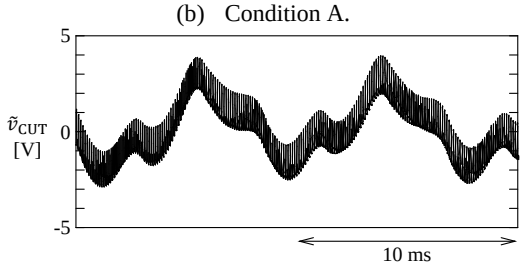

(b) Condition B: ESR increase of 150 mΩ.

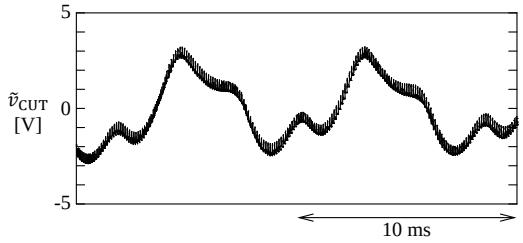

(c) Condition C: Capacitance decrease of 100 μF.

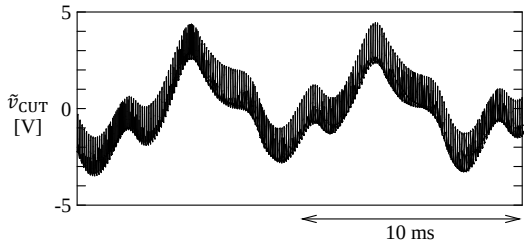

(d) Condition D: ESR increase of 150 mΩ and Capacitance decrease of 100 μF.

Fig. 5 Experimental waveforms of the ripple component of the capacitor voltage, $\tilde{v}_{CUT}$.

3.2 Procedure of the condition monitoring

Fig. 3 shows the procedure of the proposed condition monitoring method. The fast Fourier transform (FFT) is used for extracting $I_{\mathrm{CUT}}(\omega_k)$ and $V_{\mathrm{CUT}}(\omega_k)$. Plotting $Z_{\mathrm{CUT}}(\omega_k)$ at each frequency gives an impedance profile. Introducing a fitting curve by the least squares method makes it possible to obtain the capacitance and ESR. Since the method is available without disconnecting the capacitor, it can be implemented online.

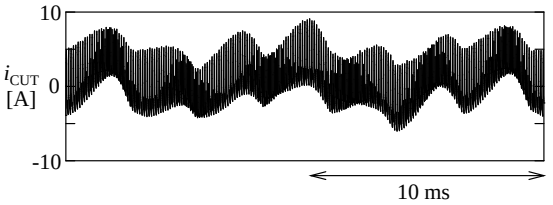

(a) Condition A.

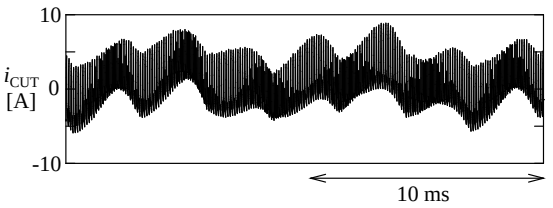

(b) Condition B: ESR increase of 150 mΩ.

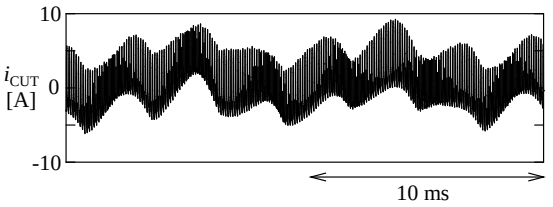

(c) Condition C: Capacitance decrease of 100 μF.

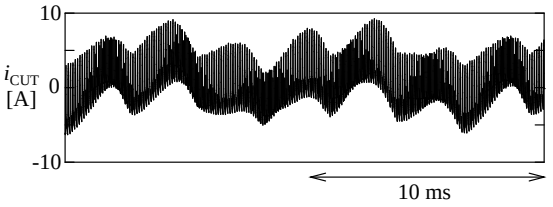

(d) Condition D: ESR increase of 150 mΩ and Capacitance decrease of 100 μF.

Fig. 6 Experimental waveforms of the ripple current i_{CUT}.

Fig. 4 illustrates a variation of the impedance profile. An increase in ESR brings a larger offset value, whereas a decrease in capacitance results in a larger value in a low-frequency region.

Although this method brings a computer burden because of using FFT, low-cost microprocessor boards, like Raspberry Pi and Arduino, are available. In addition, this method does not require a fast computation time because the ageing of capacitors progresses of the order of 100 hours.

Note that the equivalent series inductance (ESL) of the capacitor has an influence on the impedance profile. In practice, however, this influence appears only in a high-frequency region. Hence, bandwidth

Table I Ratings and circuit parameters of the three-phase inverter

System Power rating	P	1.5 kVA
AC current rating	I_S	5.8 A
AC voltage rating	V_S	150 V
Line frequency	fs	60 Hz
DC inductor	L_{DC}	2.5 mH (6.3%)
Load inductor	L_L	4 mH (12.5%)
Load resistor	R_L	10 Ω
Carrier frequency	f_C	10 kHz
Output frequency	f_O	50 Hz
Capacitors under test	C_{UT}	1100 or 1000 μF
Unit capacitance constant of the capacitors [18]	H_{CUT}	15.0 ms (1100 μF) 13.7 ms (1100 μF)

limitation makes it possible to eliminate the influence.

4. Experimental results

4.1 Experimental Conditions

This paper introduces the following conditions for the capacitor under test, C_{UT}:

- Condition A: C_{UT} = 1100 μF.
- Condition B: C_{UT} = 1100 μF with an intentionally-connected series resistance of 150 mΩ, which shows the effect of an increase in ESR.
- Condition C: C_{UT} = 1000 μF, which indicates the effect of a decrease in capacitance.
- Condition D: C_{UT} = 1000 μF with an intentionally-connected series resistance of 150 mΩ, which indicates both the effects of a decrease in capacitance and an increase in ESR.

Aluminum electrolytic capacitors with the rated voltage of 350 V were used in all the conditions.

Table I summarizes circuit parameters and ratings of the three-phase PWM inverter.

4.2 Experimental Waveforms

Fig. 5 shows the ripple component of the capacitor voltage, $\tilde{v}_{CUT}$, which was obtained from the output of the dc blocking filter. In Fig. 5 (b), the amplitude of $\tilde{v}_{CUT}$ was larger than that in Fig. 5(a), where the carrier-frequency component especially increased. This is because the capacitance had a lower impedance at the carrier frequency (14 mΩ at 10 kHz) than the series resistance of 150 mΩ. Thus, the carrier-frequency component was almost determined by the resistance. In Fig. 5(c), the amplitude of $\tilde{v}_{CUT}$ was also larger than that in Fig. 5(a), in which $2\omega_S$ and $6\omega_S$ components increased due to the decrease in capacitance.

Fig. 6 shows the ripple current i_{CUT}. All the waveforms were almost the same unlike the capacitor voltage because the ripple current provided by the inverter act as a current source [13]. The ripple current flowing out of the diode rectifier also behaved as a current source because of the dc inductor L_{DC}.

4.3 Impedance Profile

Fig. 7 shows impedance profiles obtained from FFT results of $\tilde{v}_{CUT}$ and i_{CUT} in a wide frequency range including $2\omega_S$ (120 Hz), $6\omega_S$ (360 Hz), the carrier frequency (10 kHz), and its multiples. In Fig. 7(a), the capacitance obtained from the fitting curve well agreed with C_{UT} = 1100 μF. In Fig. 7(b), the ESR increased by 199 mΩ that was almost same as the intentionally-connected resister. In Fig. 7(c), the capacitance decreased due to the smaller capacitance of C_{UT} = 1100 μF. In Fig. 7(d), both the capacitance and ESR were changed.

These results confirmed that the monitoring method obtained both the capacitance and ESR changes.

5. Conclusion

This paper has proposed a condition monitoring method of a dc-link capacitor used in a three-phase PWM inverter with a front-end diode rectifier. Experimental results confirmed that the proposed method independently extracts the capacitance and ESR. This will bring accurate lifetime estimation of dc-link capacitors.

References

[1] H. Wang and F. Blaabjerg, "Reliability of capacitors for dc-link applications in power electronic converters—an overview," IEEE Trans. Ind. Appl. vol. 50, no. 5, pp. 3569-3578, 2014.

[2] S. Yang, A. Bryant, P. Mawby, D. Xiang, L. Ran, and P. Tavner, "An Industry-Based Survey of Reliability in Power Electronic Converters," IEEE Trans. Ind. Appl., vol. 47, no. 3, pp. 1441-1451, May/Jun. 2011.

[3] K. Harada, A. Katsuki, and M. Fujiwara, “Use of ESR for deterioration diagnosis of electrolytic capacitor,” IEEE Trans. Power Electron., vol. 8, no. 4, pp. 355-361, Oct. 1993.
[4] P. Venet, F. Perisse, M. H. El-Husseini, and G. Rojat, “Realization of a smart electrolytic capacitor circuit,” IEEE Ind. Appl. Mag., vol. 8, no. 1, pp. 16–20, Jan./Feb. 2002.
[5] K. Abdennadher, P. Venet, G. Rojat, J. M. Retif, and C. Rosset, “A Real-Time Predictive-Maintenance System of Aluminum Electrolytic Capacitors Used in Uninterrupted Power Supplies,” IEEE Trans. Ind. Appl. vol. 46, no. 4, pp. 1644-1652, Jul./Aug., 2010.
[6] X.-S. Pu, T.H. Nguyen, D.-C. Lee, K.-B. Lee, and J.-M. Kim, “Fault Diagnosis of DC-Link Capacitors in Three-Phase AC/DC PWM Converters by Online Estimation of Equivalent Series Resistance,” IEEE Trans. Ind. Electron., vol. 60, no. 9, pp. 4118-4127, Sep. 2012.
[7] H. Soliman, H. Wang, and F. Blaabjerg, “A Review of the Condition Monitoring of Capacitors in Power Electronic Converters,” IEEE Trans. Ind. Appl., vol. 52, no. 6, pp. 4976-4989, Jul. 2016.
[8] P. Sun, C. Gong, X. Du, Q. Luo, H. Wang. L. Zhou, ”Online Condition Monitoring for Both IGBT Module and DC-Link Capacitor of Power Converter Based on Short-Circuit Current Simultaneously,” IEEE Trans. Ind. Electron., vol. 64, no. 5, pp. 3662-3671, Jan. 2017.
[9] E. Farjar, H. Givi, and T. Ghanbari, ”Application of an Efficient Rogowski Coil Sensor for Switch Fault Diagnosis and Capacitor ESR Monitoring in Nonisolated Single-Switch DC–DC Converters,” IEEE Trans. Power Electron., vol. 32, no. 2, Apr. 2016.
[10] U. M. Choi, F. Blaabjerg, and F. Iannuzzo ”Advanced power cycler with intelligent monitoring strategy of IGBT module under test,” Microelectron. Rel. vol. 76-77, pp. 522-526, Sep. 2017.
[11] N. Agarwal, M.W. Ahmad, and S. Anand, ”Quasi-Online Technique for Health Monitoring of Capacitor in Single-Phase Solar Inverter,” IEEE Trans. Power Electron. Vol. 33, no. 6, pp. 5283 – 5291, Jun. 2018.
[12] M. Makdessi, A. Sari, P. Venet, G. Aubard, F. Chevailier, R. Preseau, T. Doytchinov and J. Duwattez, “Lifetime estimation of high-temperature high-voltage polymer film capacitor based on capacitance loss,” Microelectron. Rel.., vol. 55, no. 9-10, pp. 2012-2016, 2015.
[13] H. Wang, D. A. Nielsen, and F. Blaabjerg, “Degradation testing and failure analysis of DC film capacitors under high humidity conditions,” Microelectron. Rel., vol. 55, no. 9-10, pp. 2007-2011, 2015.
[14] M. Makdessi, A. Sari, P. Venet, G. Aubard, F. Chevailier, R. Preseau, T. Doytchinov and J. Duwattez, “Lifetime estimation of high-temperature high-voltage polymer film capacitor based on capacitance loss,” Microelectron. Rel.., vol. 55, no. 9-10, pp. 2012-2016,

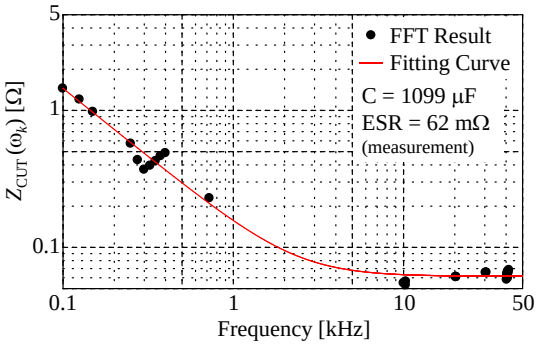

(c) Condition A.

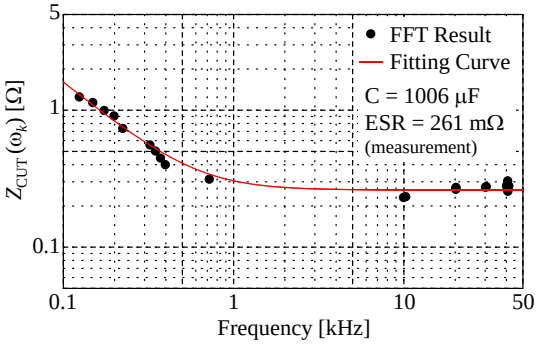

(b) Condition B: ESR increase of 150 mΩ.

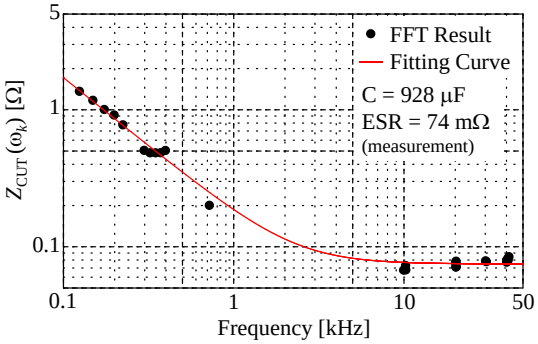

(c) Condition C: Capacitance decrease of 100 μF.

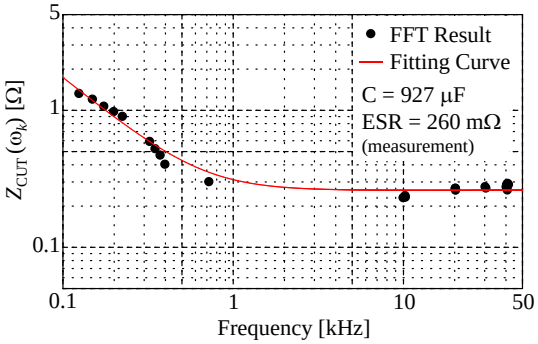

(d) Condition D: ESR increase of 150 mΩ and Capacitance decrease of 100 μF.

Fig. 7 Experimental results of impedance profiles.

2015.
[15] D. Zhou, H. Wang, F. Blaabjerg, S.K. Kaer, and D. Blom-Hansen, “Degradation Effect on Reliability Evaluation of Aluminum Electrolytic Capacitor in Backup Power Converter,” IEEE IFEEC, pp. 202-207, 2017.
[16] K. Hasegawa, K. Tsuzaki, and S. Nishizawa, “DC-bias-voltage dependence of degradation of aluminum electrolytic capacitors,” Microelectron. Rel., vol. 83, pp. 115-118, 2018.
[17] K. Hasegawa, I. Omura, and S. Nishizawa, “An Evaluation Circuit for DC-Link Capacitors Used in a High-Power Three-Phase Inverter with Condition Monitoring,” IEEJ/IEEE Intl. Power Electron. Conf.,pp.1938-1942, May 2018.
[18] H. Fujita, S. Tominaga, and H. Akagi, “Analysis and design of a dc voltage-controlled static var compensator using quad-series voltage-source inverters,” IEEE Trans. Ind. Appl., vol. 32, no. 4, pp. 970--977, 1996.